

Deformable 2-D Template Matching Using Orthogonal Curves

Hemant D. Tagare, *Member, IEEE*

Abstract— In this paper a new formulation of the two-dimensional (2-D) deformable template matching problem is proposed. It uses a lower-dimensional search space than conventional methods by precomputing extensions of the deformable template along orthogonal curves. The reduction in search space allows the use of dynamic programming to obtain globally optimal solutions and reduces the sensitivity of the algorithm to initial placement of the template. Further, the technique guarantees that the result is a curve which does not collapse to a point in the absence of strong image gradients and is always nonself intersecting. Examples of the use of the technique on real-world images and in simulations at low signal-to-noise ratios (SNR's) are also provided.

Index Terms—Active contours, segmentation, template matching.

I. INTRODUCTION

INTERACTIVE template matching is the first step in quantitative analysis of many medical images. Most interactive template matching algorithms require the user to place a template (a closed curve) approximately in the right position and orientation. Then the algorithm systematically adapts the template to fit the image gradient.

The template contains prior geometric information about the organ which is being segmented. Many studies can be analyzed by maintaining a database of a few useful templates [4], [18]. For those images where the shape of an organ does not conform to the prior information, active contour algorithms such as “snakes” [8] can be used.

During the template fitting stage of a deformable template algorithm, the deformed template is parameterized as a curve $C : t \rightarrow (x(t), y(t))$ (t is not necessarily the arc length), external and internal energies are associated with it, and functions $x_o(t), y_o(t)$ are sought which minimize a weighted sum of the internal and external energies [2], [8], [11], [17], [22], [23]. The energies associated with the curve C are of the form

$$E(C) = \int \Gamma(x, y, \dot{x}, \dot{y}, \dots, x^{(n)}, y^{(n)}) dt. \quad (1)$$

Quite often only the image of the optimal curve is of interest and its parameterization is irrelevant. The external and internal energies of such curves are formulated to be independent of

Manuscript received August 12, 1994; revised May 23, 1996. This work was supported by the National Library of Medicine under Grant 1-R01-LM05007. The Associate Editor responsible for coordinating the review of this paper and recommending its publication was M. Viergever.

The author is with the Departments of Diagnostic Radiology and Electrical Engineering, Yale University, New Haven, CT 06520 USA (e-mail: tagare@cs.yale.edu).

Publisher Item Identifier S 0278-0062(97)00981-6.

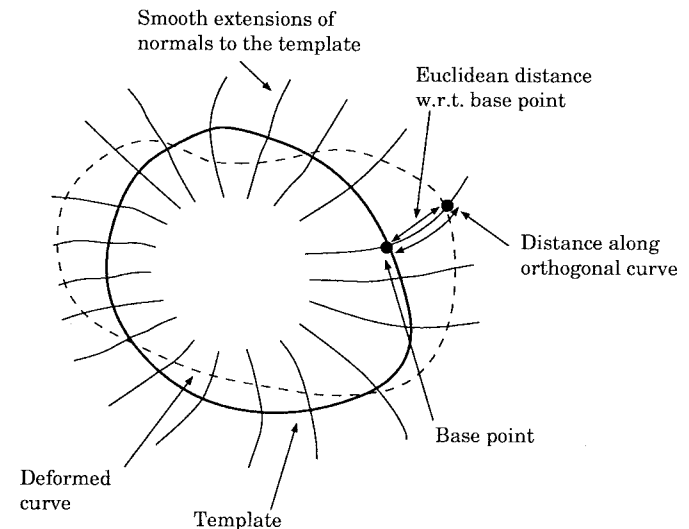


Fig. 1. Smooth orthogonal curves.

the parameterization. For such energies, it can be shown (see Appendix) that if the optimal deformation is small, then it need be only normal to the template.

The main aim of this paper is to extend the strategy of deforming the template along normals over larger regions while avoiding singular points (points at which the extended normals intersect). The key idea, which is illustrated in Fig. 1, is to extend the normals as curves rather than as straight lines. These curves are perpendicular to the template and are called *orthogonal curves*. Given the orthogonal curves, the template is deformed by restricting every point on the template to move only along its orthogonal curve. The resulting deformation of the template is uniquely identified by a single function which expresses the distance that each point of the template moves along its orthogonal curve.

If the template is constructed beforehand, then the orthogonal curves can be precomputed. Precomputing the orthogonal curves and using them to deform the template has a number of advantages. First, every deformation is defined by a single function, so the optimization procedure uses a smaller search space. It is often feasible to find the global minimum. In contrast, deformations in conventional techniques are defined by a pair of functions and have a much bigger search space.

Second, using orthogonal curves it is easy to express the prior knowledge that smoothly deformed shapes close to the template are more desirable than jagged shapes which are farther away from the template. The prior is formulated as a sum of proximity and smoothness energies. Since each

orthogonal curve intersects the template at a single point (called the base point of the orthogonal curve, Fig. 1), the proximity of the deformed point to the template is defined as the Euclidean distance between it and the corresponding base point. The smoothness of the deviation is defined as the change of the Euclidean distance along the deformed curve. The exact formulations are given in Section III.

Third, by controlling the amount of extension from the template, explicit control over the region of deformation can be obtained.

Finally, the curve resulting from the deformation is guaranteed to be closed and nonself intersecting.

The use of orthogonal curves has some limitations. Since orthogonal curves decrease the degrees of freedom used to deform the template (by using one function rather than two), in theory, the set of possible deformations of the template is smaller. Restriction to a smaller set of possible deformations is not a major limitation in processing medical images since templates with simple shapes fit a large variety of medical objects. For example, in [18], deformations of a single circular template along radial directions were successfully used to obtain a number of outlines of wrist bones in computed tomography (CT) images. The study [4] also used deformations of a single circular template to model a number of anatomical objects in medical images.

In the computer vision literature, search along normals has been used in a number of algorithms, for example, it is used in rigid-template-matching algorithms to estimate the location and pose of an object [9]. It is also used in registration of images obtained from different modalities [6], [14]. The algorithm presented in this paper can be viewed as an extension of these algorithms to nonrigid templates and to larger regions of convergence.

An initial version of the current algorithm was reported in [18]. It relied exclusively on a circular template and a heuristic was used to guarantee closure of the deformed curve. Both of these restrictions are removed in the algorithm presented here.

II. TEMPLATES, ORTHOGONAL CURVES, AND THE DEFORMED CURVE

In this section, we define orthogonal curves and use them to find an expression for the deformed curve. An intermediate step, which shows that orthogonal curves exist for any template, is postponed till Section IV.

Suppose that the template is a closed curve C which does not intersect itself. In a coordinate frame attached to the template, the template is described by its arc length parameterization $C : \theta \rightarrow (x(\theta), y(\theta))$. Further suppose that the region over which the template can be deformed is bounded by two curves C_{in} and C_{out} , where C_{in} is located inside C and C_{out} is located outside C (Fig. 2).

Let R_θ be the orthogonal curve passing through the base point $(x(\theta), y(\theta))$ on the template. We assume the following:

- 1) Each R_θ begins on the curve C_{in} , orthogonally intersects C at the base point, and ends at the curve C_{out} .
- 2) Each R_θ has a continuous tangent.
- 3) No two orthogonal curves intersect.

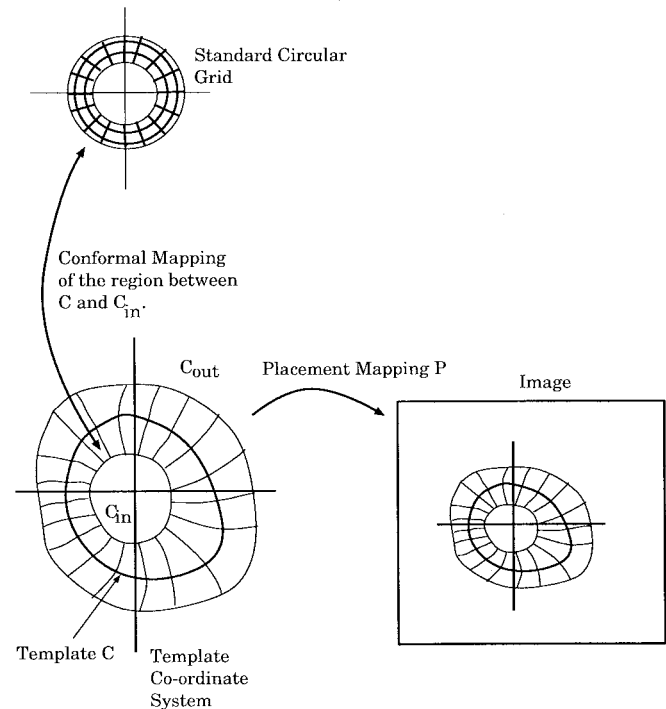


Fig. 2. Region of deformation in template and image coordinates.

If R_θ is parameterized by its arc length r (which is zero at the base point of R_θ , increases as R_θ proceeds outwards, and decreases as R_θ proceeds inwards), then R_θ can be written in the template coordinate system as

$$R_\theta : r \rightarrow \begin{pmatrix} x(\theta) + \Delta x_\theta(r) \\ y(\theta) + \Delta y_\theta(r) \end{pmatrix}$$

where the functions $\Delta x_\theta(r)$ and $\Delta y_\theta(r)$ give the position of R_θ with respect to the base point and $(\Delta x_\theta(0), \Delta y_\theta(0)) = (0, 0)$.

If the template is deformed into a curve C^* by moving template points along the orthogonal curves, then C^* is given by

$$C^* : \theta \rightarrow \begin{pmatrix} x(\theta) + \Delta x_\theta(r(\theta)) \\ y(\theta) + \Delta y_\theta(r(\theta)) \end{pmatrix}$$

where $r(\theta)$ gives the displacements of the template points along the orthogonal curves.

The placement of the template on the image is given by a mapping from the template coordinate system to the image coordinate system. We assume that the template is placed on the image by a translation and rotation. Hence, the set of curves in the image obtained by deforming the template can be expressed as

$$C^* : \theta \rightarrow \begin{pmatrix} x_I(\theta) \\ y_I(\theta) \end{pmatrix} = R \begin{pmatrix} x(\theta) + \Delta x_\theta(r(\theta)) \\ y(\theta) + \Delta y_\theta(r(\theta)) \end{pmatrix} + T \quad (2)$$

where $(x_I(\theta), y_I(\theta))$ are the coordinates of C^* in the image coordinate frame, R is a rotation matrix, and T is the translation vector.

From (2) it is easy to show that any C^* is closed and nonself intersecting.

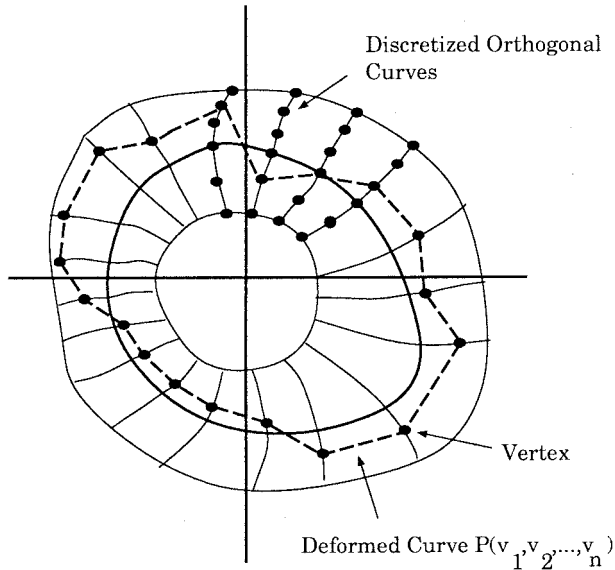


Fig. 3. Discrete orthogonal curves.

A. Discrete Orthogonal Curves

Discrete versions of orthogonal and deformed curves are used in formulation of template matching. The family of orthogonal curves is discretized by sampling the template curve uniformly along the arc length at N base points. From each of the base points the orthogonal curves are traced inwards and outwards and each orthogonal curve is sampled uniformly along its arc length at $2M + 1$ points (Fig. 3).

The points thus obtained are denoted by $\mathbf{x}_{i,j}$, $i = 1, \dots, N$, and $j = -M, \dots, M$ (Fig. 3). The index i refers to the orthogonal curve that the point belongs to, and the index j refers to the location along the orthogonal curve. All points $\mathbf{x}_{i,j}$ belong to the i th orthogonal curve and the base point of the i th orthogonal curve is $\mathbf{x}_{i,0}$.

When the template and the orthogonal curves are placed on the image, $\mathbf{x}_{i,j}$ are transformed into points on the image by

$$\tilde{\mathbf{x}}_{i,j} = R\mathbf{x}_{i,j} + T \quad (3)$$

where R and T are the rotation matrix and the translation vector.

The deformed curve is discretized as an N -sided polygon (Fig. 3). The k th vertex of the polygon, \mathbf{v}_k , is constrained to lie on the k th orthogonal curve

$$\mathbf{v}_k \in \{\tilde{\mathbf{x}}_{k,j}, j = -M, \dots, M\}. \quad (4)$$

The entire polygon is denoted by $P(\mathbf{v}_1, \mathbf{v}_2, \dots, \mathbf{v}_N)$.

Below, to simplify the equations for the energy we refer to the first vertex as the vertex \mathbf{v}_1 and also as \mathbf{v}_{N+1} . Similarly, we refer to the first base point as $\tilde{\mathbf{x}}_{1,0}$ and also as $\tilde{\mathbf{x}}_{N+1,0}$.

III. INTERNAL AND EXTERNAL ENERGIES

The internal energy associated with the deformed curve is the weighted sum of a proximity energy and a smoothness energy.

The proximity energy $I_1(P)$ measures the displacements of the vertices from the base points

$$I_1(P(\mathbf{v}_1, \dots, \mathbf{v}_N)) = \sum_{k=1}^N D(\mathbf{v}_k - \tilde{\mathbf{x}}_{k,0}) \quad (5)$$

where $D(\cdot)$ is the Euclidean distance.

The smoothness energy $I_2(P)$ measures the dissimilarity of distances of consecutive vertices from their base points

$$I_2(P(\mathbf{v}_1, \dots, \mathbf{v}_N)) = \sum_{k=1}^N |D(\mathbf{v}_{k,j} - \tilde{\mathbf{x}}_{k,0}) - D(\mathbf{v}_{k+1} - \tilde{\mathbf{x}}_{k+1,0})|. \quad (6)$$

The external energy $X(P)$ is the net component of the image gradient along the outward pointing normals of each side of the polygon, i.e.

$$X(P(\mathbf{v}_1, \dots, \mathbf{v}_N)) = \delta \sum_{k=1}^N L_k \int_0^1 \mathbf{n}_k \cdot \nabla I(\alpha \mathbf{v}_k + (1 - \alpha) \mathbf{v}_{k+1}) d\alpha \quad (7)$$

where \mathbf{n}_k is the outwards pointing normal and L_k is the length of the side joining vertex \mathbf{v}_k to \mathbf{v}_{k+1} . The integrand in the above expression is the inner product between the outwards normal and the image gradient. The constant δ is set to $+1$ if we seek a dark to white transition along the outwards normal and -1 for a white to dark transition.¹

The net energy associated with the deformed curve is given by

$$E(P(\mathbf{v}_1, \dots, \mathbf{v}_N)) = -\rho_1 X(P(\mathbf{v}_1, \dots, \mathbf{v}_N)) + \rho_2 I_1(P(\mathbf{v}_1, \dots, \mathbf{v}_N)) + \rho_3 I_2(P(\mathbf{v}_1, \dots, \mathbf{v}_N)) \quad (8)$$

where the ρ 's are nonnegative weights.

Given an image and a template with its orthogonal curves, we seek the deformed curve that minimizes the net energy. This is the formulation of a deformable template matching problem using orthogonal curves.

IV. ORTHOGONAL CURVES AND CONFORMAL MAPS

Before we proceed to seek an algorithm that gives the optimum deformation, we settle the existence of orthogonal curves. We do this for the continuous case. The discrete case is just a finite sampling of the continuous case.

We begin by considering a specific recipe for generating orthogonal curves. The key idea is to imagine C_{in} , C , and C_{out} as contours of a two dimensional (2-D) function which is continuous in the region between C and C_{in} and also between C and C_{out} ; and to realize that the gradient trajectories of the function are orthogonal to the contours everywhere and therefore are admissible as orthogonal curves.

More precisely, consider the region between C_{in} and C . Suppose we have a function $\phi(x, y)$ defined in this region

¹The external energy can be easily modified if the nature of the transition (white-to-dark or dark-to-white) is not known by using the magnitude of ∇I from \mathbf{v}_k to \mathbf{v}_{k+1} instead of the component of ∇I along the normal. This change does not alter the algorithm.

such that

$$\begin{aligned}\phi(x, y) &= c_1, \text{ on } C_{\text{in}} \\ \phi(x, y) &= c_2, \text{ on } C\end{aligned}\quad (9)$$

with $c_1 > c_2$. If $\phi()$ has well-defined gradients, then the gradient direction at any point is given by $\mathbf{n}(x, y) = \frac{\nabla\phi(x, y)}{\|\nabla\phi(x, y)\|}$. Starting from a base point $(x(\theta), y(\theta))$ on the template, the gradient trajectory $t \rightarrow (x(t), y(t))$ is given by the solution of the coupled differential equations

$$\frac{d}{dt} \begin{pmatrix} x(t) \\ y(t) \end{pmatrix} = \mathbf{n}(x(t), y(t)) \quad (10)$$

with the boundary condition

$$\begin{pmatrix} x(0) \\ y(0) \end{pmatrix} = \begin{pmatrix} x(\theta) \\ y(\theta) \end{pmatrix}. \quad (11)$$

By construction, this trajectory is orthogonal to C and is admissible as an orthogonal curve extending inwards from C . By repeating this procedure for all points of C , the entire set of orthogonal curves extending inwards from C can be obtained.

If there exists more than one $\phi()$ which can give curves that are orthogonal to C , we would like to use the smoothest. Measuring the smoothness of $\phi()$ by $\int \int \|\nabla\phi(x, y)\|^2 dx dy$, the smoothest $\phi()$ is given as the solution to the corresponding Euler–Lagrange equation, $\nabla^2\phi(x, y) = 0$ with the boundary conditions of (9).

Therefore, $\phi()$ is a harmonic function within the region bounded by C_{in} and C . From harmonic function theory, we know that the gradient trajectories of $\phi()$ may be thought of as contours of the conjugate harmonic function. Furthermore, the function $\phi()$ and the conjugate harmonic function define a conformal mapping of the region between C and C_{in} on to an annulus (Fig. 2).

The existence of such a conformal map for any closed nonintersecting curves C and C_{in} is guaranteed by the theory of conformal mappings [7], [13]. It is also known that the conformal mapping is nonsingular in the region of interest and the inverse map exists, is conformal, and nonsingular. If a standard circular grid is created in the annulus, the image of the grid under the inverse conformal map gives an orthogonal grid in the template space such that the inner and outer circles of the annulus are mapped onto C_{in} and C . The image of the radial grid lines are the desired orthogonal curves between C_{in} and C .

This argument applied to the region between C_{out} and C gives orthogonal curves in that region. Since the mappings are conformal, the two sets of orthogonal curves are guaranteed to be normal to C at all points. Therefore, the orthogonal curves in the two regions can be joined at C to obtain curves that have a continuous tangent vectors and extend from C_{in} to C_{out} .

This establishes the existence of orthogonal curves for a general template C .

The numerical procedure for obtaining the grid directly follows from the above discussion. First, the harmonic equation is solved between C_{in} and C and independently between C and C_{out} by a standard finite-difference successive-overrelaxation method. As mentioned before, N points are placed uniformly along C and from each point the inwards and outwards gradient trajectories are obtained by solving (10) by finite

TABLE I
PARTIAL ENERGY FUNCTIONS AND THEIR MINIMA

Partial Energy Functional	Minimizing Set
$\mathcal{E}_1 = \phi(\mathbf{v}_1, \mathbf{v}_2) + \phi(\mathbf{v}_2, \mathbf{v}_3^*)$	$\{\mathbf{v}_2^*\}$
$\mathcal{E}_2 = \phi(\mathbf{v}_1, \mathbf{v}_2) + \phi(\mathbf{v}_2, \mathbf{v}_3) + \phi(\mathbf{v}_3, \mathbf{v}_4^*)$	$\{\mathbf{v}_2^*, \mathbf{v}_3^*\}$
$\mathcal{E}_3 = \phi(\mathbf{v}_1, \mathbf{v}_2) + \phi(\mathbf{v}_2, \mathbf{v}_3) + \phi(\mathbf{v}_3, \mathbf{v}_4) + \phi(\mathbf{v}_4, \mathbf{v}_5^*)$	$\{\mathbf{v}_2^*, \mathbf{v}_3^*, \mathbf{v}_4^*\}$

differences. The two curves are joined at the base point and the combined curve is uniformly sampled at $2M + 1$ points.

V. OPTIMIZATION

We return to the problem of minimizing the net energy and observe that the energy in (8) can be written as

$$E(P(\mathbf{v}_1, \dots, \mathbf{v}_N)) = \sum_{k=1}^N \phi(\mathbf{v}_k, \mathbf{v}_{k+1}) \quad (12)$$

where $\phi()$ is

$$\begin{aligned}\phi(\mathbf{v}_k, \mathbf{v}_{k+1}) &= -\rho_1 \delta L_k \int_0^1 \mathbf{n}_k \cdot \nabla I(\alpha \mathbf{v}_k + (1 - \alpha) \mathbf{v}_{k+1}) d\alpha \\ &\quad + \rho_2 D(\mathbf{v}_k - \tilde{\mathbf{x}}_{k,0}) \\ &\quad + \rho_3 |D(\mathbf{v}_k - \tilde{\mathbf{x}}_{k,0}) - D(\mathbf{v}_{k+1} - \tilde{\mathbf{x}}_{k+1,0})|.\end{aligned}\quad (13)$$

Since E has this form, its global minimum can be found by using dynamic programming. To illustrate this, consider the case for $N = 5$, where

$$\begin{aligned}E(P(\mathbf{v}_1, \dots, \mathbf{v}_5)) &= \phi(\mathbf{v}_1, \mathbf{v}_2) + \phi(\mathbf{v}_2, \mathbf{v}_3) \\ &\quad + \phi(\mathbf{v}_3, \mathbf{v}_4) + \phi(\mathbf{v}_4, \mathbf{v}_5) + \phi(\mathbf{v}_5, \mathbf{v}_1).\end{aligned}\quad (14)$$

Suppose we fix \mathbf{v}_1 and find that $\mathbf{v}_2^*, \dots, \mathbf{v}_5^*$ give the minimum E for that choice of \mathbf{v}_1 . From the form of E and the dynamic programming principle we know that each partial energy on the left-hand side of Table I is minimized by the set on the right-hand side of the table. Hence, for a given \mathbf{v}_1 , we may proceed to find the minimum as follows.

- 1) For every \mathbf{v}_3 , tabulate the \mathbf{v}_2 that minimizes \mathcal{E}_1 .
- 2) For every \mathbf{v}_4 , tabulate the \mathbf{v}_3 that minimizes $\mathcal{E}_2 = \phi(\mathbf{v}_3, \mathbf{v}_4) + \min_{\mathbf{v}_2, \mathbf{v}_3} \mathcal{E}_1$ where $\min_{\mathbf{v}_2, \mathbf{v}_3} \mathcal{E}_1$ is the minimum value of \mathcal{E}_1 with respect to \mathbf{v}_2 for a given \mathbf{v}_3 .
- 3) For every \mathbf{v}_5 , tabulate the \mathbf{v}_4 that minimizes $\mathcal{E}_3 = \phi(\mathbf{v}_5, \mathbf{v}_4) + \min_{\mathbf{v}_3, \mathbf{v}_4} \mathcal{E}_2$.
- 4) Find the \mathbf{v}_5 that minimizes $E = \phi(\mathbf{v}_5, \mathbf{v}_1) + \min_{\mathbf{v}_4, \mathbf{v}_5} \mathcal{E}_3$. This is the optimum \mathbf{v}_5 for the given \mathbf{v}_1 , and the values of $\mathbf{v}_2, \dots, \mathbf{v}_4$ that minimize $\mathcal{E}_3, \dots, \mathcal{E}_1$ for the optimal value of \mathbf{v}_5 give the optimal deformation.

Repeating the above procedure for different values of \mathbf{v}_1 gives the global minimum.

The algorithm used in the general case is a straightforward extension of the above.

- 1) Select a \mathbf{v}_1 from the set $\{\tilde{\mathbf{x}}_{1,j}, j = -M, \dots, M\}$.
- 2) For the given \mathbf{v}_1 , tabulate the value of $\mathbf{v}_2 \in \{\tilde{\mathbf{x}}_{2,j}, j = -M, \dots, M\}$ that minimizes the partial energy

$$\mathcal{E}_1 = \phi(\mathbf{v}_1, \mathbf{v}_2) + \phi(\mathbf{v}_2, \mathbf{v}_3)$$

for every $\mathbf{v}_3 \in \{\tilde{\mathbf{x}}_{3,j}, j = -M, \dots, M\}$.

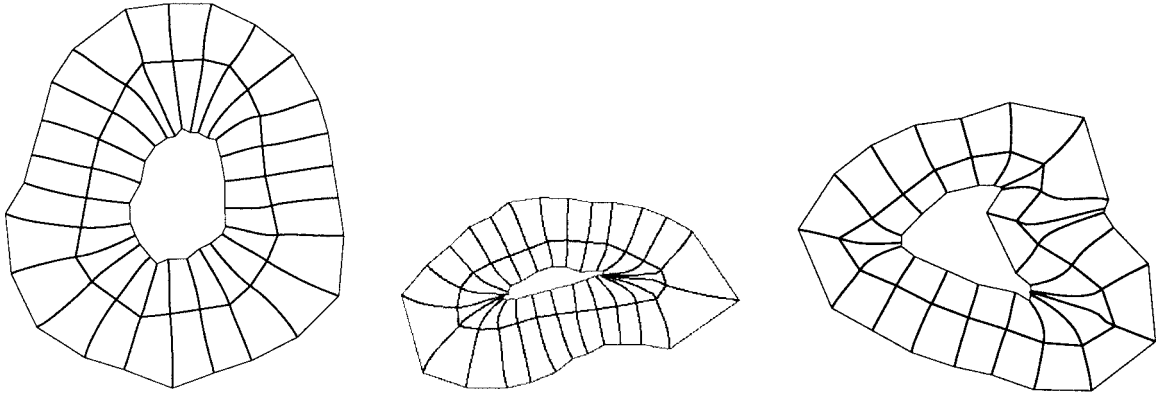


Fig. 4. Some templates and orthogonal curves.

- 3) For all $k, 3 \leq k < N$, tabulate the $\mathbf{v}_k \in \{\tilde{\mathbf{x}}_{k,j}, j = -M, \dots, M\}$ that minimizes the partial energy \mathcal{E}_k

$$\mathcal{E}_k = \phi(\mathbf{v}_{k+1}, \mathbf{v}_k) + \min_{\mathbf{v}_{k-1}} \mathbf{v}_k \mathcal{E}_{k-1}$$

for every $\mathbf{v}_{k+1} \in \{\tilde{\mathbf{x}}_{k+1,j}, j = -M, \dots, M\}$.

- 4) Finally, evaluate the energy E for all values of $\mathbf{v}_N \in \{\tilde{\mathbf{x}}_{N,j}, j = -M, \dots, M\}$ by

$$E = \phi(\mathbf{v}_N, \mathbf{v}_1) + \min_{\mathbf{v}_{N-1}} \mathbf{v}_N \mathcal{E}_{N-1}.$$

- 5) The minimum value of E in the above set is the desired optimum value for the given \mathbf{v}_1 , and the values of $\mathbf{v}_k, k = 2, \dots, N$ which minimize the partial energies for this E give the optimally deformed curve.
- 6) Repeat steps 1)–5) for all possible values of \mathbf{v}_1 to find the global minimum and the corresponding deformed curve.

The number of evaluations of $\phi()$ in the above procedure is $O(M^3N)$. Although this may appear to be computationally expensive, it is in fact quite feasible as long as M is not excessively high. In all of the experiments reported in this paper M and N were 10 and 25, respectively, and the minima was found under 10 s. on a SUN SPARC Station 2. The time was independent of the quality of the image and the initial position of the template.

For high-resolution images, M may be large and the above dynamic programming procedure may not be feasible. In that case, either a faster dynamic programming procedure or a heuristic minimization procedure [3] can be used. Multiresolution or adaptive resolution strategies can also decrease the computational burden.

VI. EXPERIMENTAL RESULTS

First, we check that the orthogonal curve generation procedure gives usable curves for a variety of shapes. Fig. 4 shows some examples of templates, inner, outer, and orthogonal curves generated by the technique.

The next set of experiments show the results of deformable template matching. As with any variational formulation of deformable template matching or active contours [8], the appropriate weights for external and internal energy are determined after some experimentation. However, once the weights are de-

TABLE II
ALGORITHM PARAMETERS

No. of Orth. Curves (N)	25
No. of Points/ Orth. Curve ($2M + 1$)	21
Gradient Weight (ρ_1)	0.9
Proximity Weight (ρ_2)	5.0
Smoothness Weight (ρ_3)	30.0

termined two properties of the algorithm can be demonstrated by using real-world and simulated images. First, because the algorithm finds the global minima within the search space, it is relatively insensitive to the initial position of the template. Consequently, the same template can be propagated through many slices in a three-dimensional (3-D) stack to obtain boundaries of an organ. Second, since the algorithm does not get trapped in local minima, it performs well with respect to noise.

The first property is illustrated in Fig. 5. The figure shows three images from a 3-D wrist CT image (transverse distance between consecutive slices = 1.5 mm). The three images correspond to slice one, three, and five in the 3-D image stack. Fig. 6 shows the initial placement of the left-most template of Fig. 4 on the wrist CT images. Fig. 7 shows the optimally deformed curves produced by the algorithm. The values of all parameters used in the algorithm are given in Table II.

The stability of the algorithm with respect to the gradient, proximity, and smoothness weights is shown in Figs. 8–10. The stability was investigated in the following way. The three weights were changed one at a time. Each weight was decreased to 50% of the value shown in Table II and then increased to 200% of the value with the other two weights fixed. For each such combination, the optimal curve was found for slice one with the initial placement of Fig. 6. Fig. 8 shows the result with the gradient weight varied from 50% to 200%. Fig. 9 shows the result with the proximity weight varied from 50% to 200%. Fig. 10 shows the result with the smoothness weight varied from 50% to 200%. It is clear from figures that the algorithm is stable over these range of weights for this set of images.

Of course, the weights in Table II are not universally useful. Other images may require a different set of weights and the stability ranges might be different.

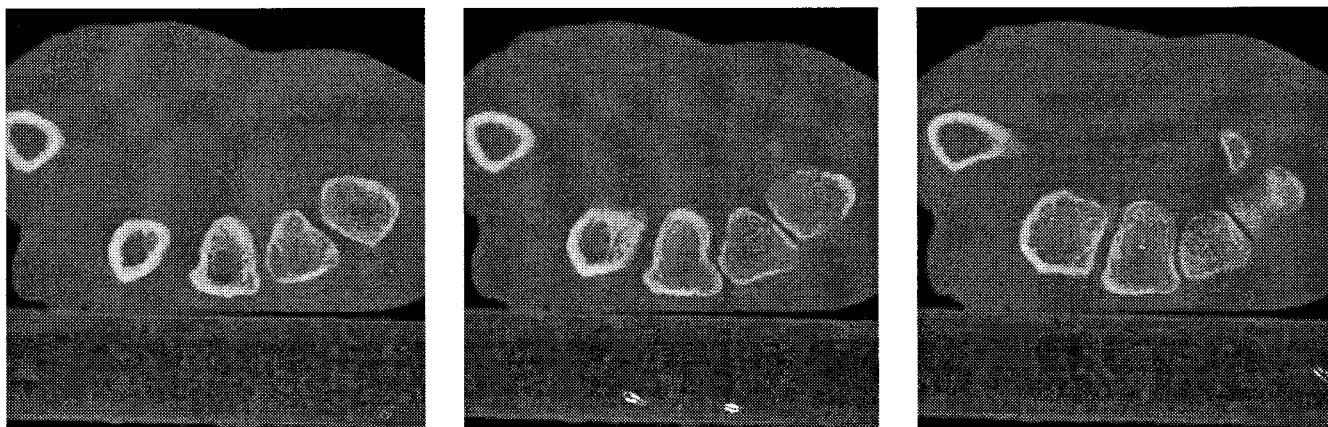


Fig. 5. Images from a 3-D wrist CT stack.

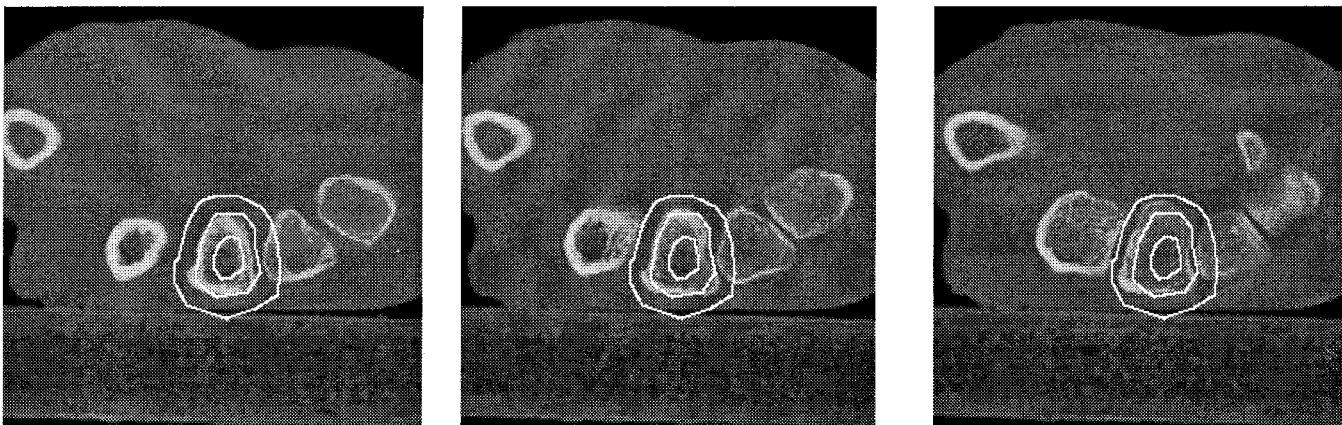


Fig. 6. Initial placement of the template.

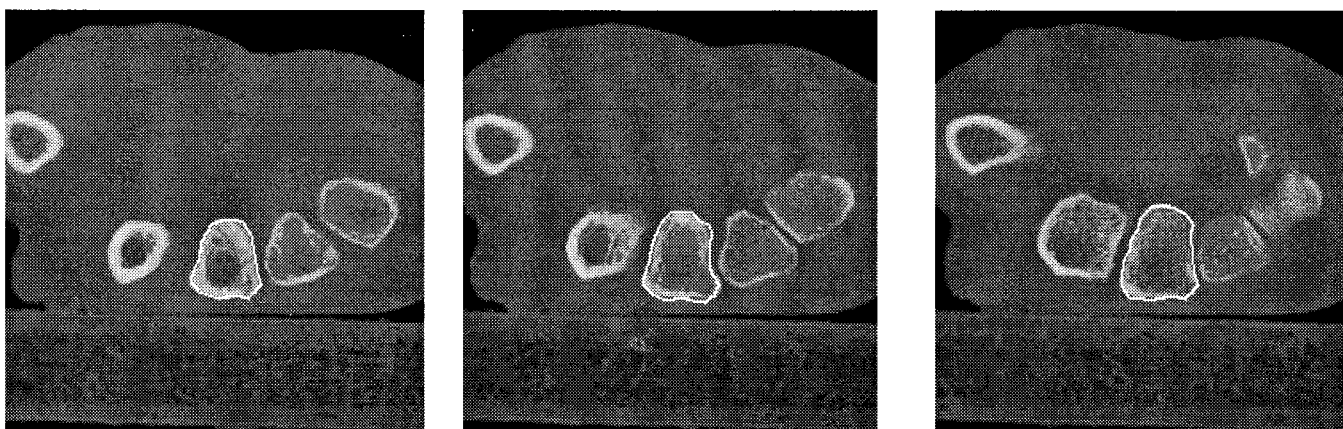


Fig. 7. The deformed template.

The algorithm has been successfully used in other modalities. Fig. 11 shows an example of the use in magnetic resonance imaging (MRI) images. The figure shows the initial placement of the middle template of Fig. 4 on a cardiac MRI image and the optimal deformed match of the template to the

aortic arch. The weights in Table II were used in this example too.

The next experiment assessed the performance of the optimization algorithm with respect to noise and placement error. The assessment is carried out by simulations. In the first

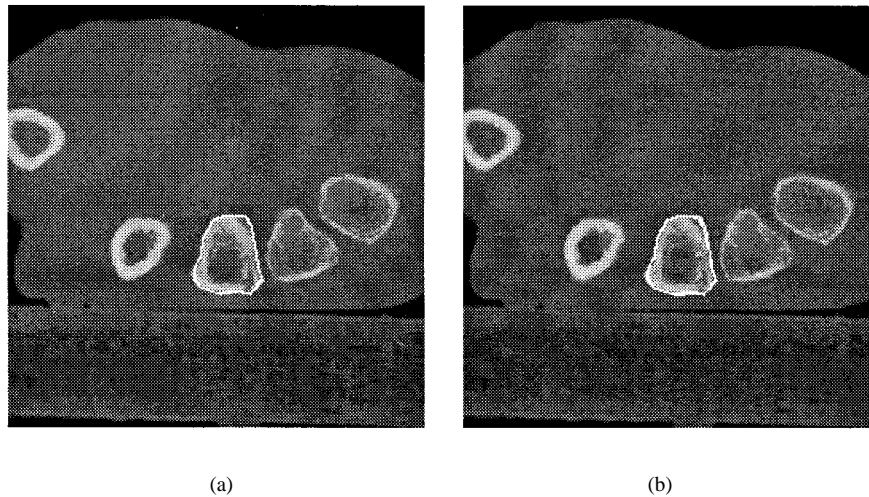


Fig. 8. Stability with respect to the gradient weight: (a) weight = 50% of nominal and (b) weight = 200% of nominal.

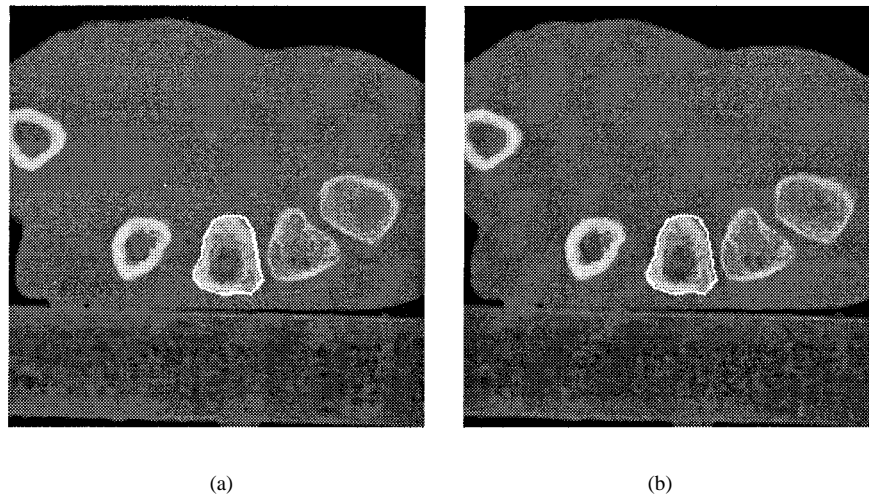


Fig. 9. Stability with respect to the proximity weight: (a) weight = 50% of nominal and (b) weight = 200% of nominal.

simulation, an image of a circle (radius = 21 pixels) with a gray level value of ten, was placed on a background of gray level zero. Gaussian noise having zero mean and standard deviations of 0.0, 1.0, 2.5, 5.0, and 10.0 was added to the image.

If the signal-to-noise ratio (SNR) is defined as $20 \cdot \log(\text{gray-level step size at the edge}/\text{noise standard deviation})$ dB then the SNR's of the simulations are ∞ , 20, 12, 6, and 0 dB.

For each value of the standard deviation, a circular template was positioned on the image and the optimal deformation sought using the algorithm of Section V. The circular template had the same radius as the circle in the image. The orthogonal curves of the circular template are radial lines. All parameters of the simulation had the same value as that shown in Table II, except that the gradient weight was set to 10.0 to compensate for the lower contrast of the circle against the background. The deformed curve obtained after optimization was compared to the original circle and the relative error in estimating the circle

was computed as

$$\text{relative error} = \frac{\text{root mean square radial error}}{\text{discretization step size in the radial direction}}$$

The root mean square radial error is simply the root mean square deviation of the deformed curve measured radially outwards from the true position of the circle in the image (Fig. 12).

The same simulation was repeated with the initial placement of the circular template shifted to the right of the true circle. Shifts of 0%, 25% and 35% of the radius were used.² Fig. 13 shows a plot of the error as a function of the SNR for different initial placements (the data are also reported in Table III). The relative error does not increase appreciably beyond the

²Note that a shift of 50% of the radius would place the boundary of the circle outside of the region of deformation of the template.

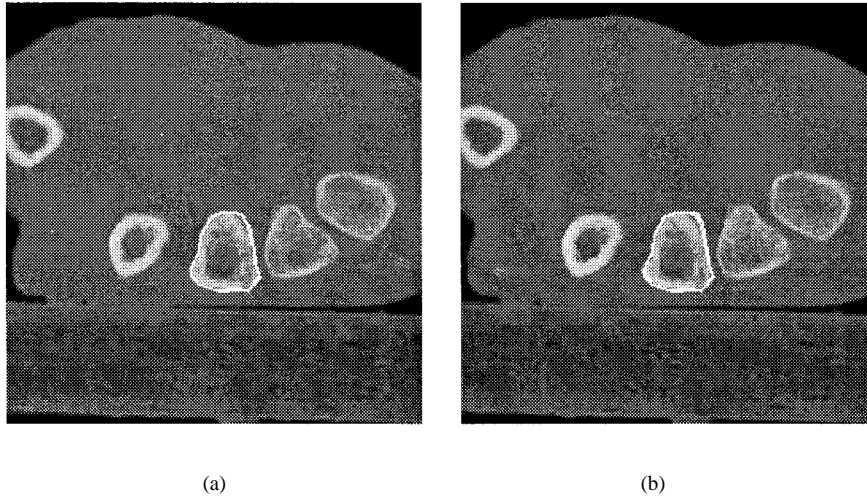


Fig. 10. Stability with respect to the smoothness weight (a) weight = 50% of nominal and (b) weight = 200% of nominal.

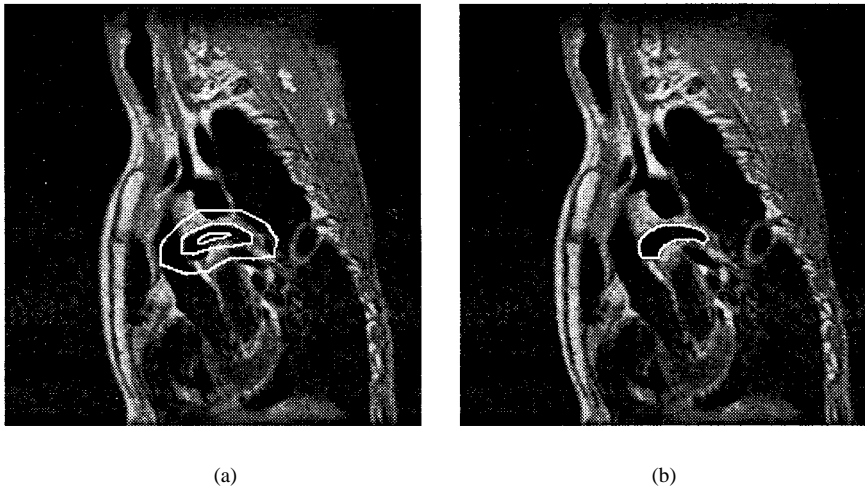


Fig. 11. Deformable template match to an MRI image.

discretization step size. The robustness of the optimal curve to initial placement is clearly seen in the figure.

VII. CONCLUSION

A new formulation of deformable 2-D template matching is proposed. The formulation uses precomputed orthogonal curves to deform the template. The optimal deformation is found by dynamic programming. The optimal curve is guaranteed to be closed and nonself intersecting.

Demonstrations and simulations show that the algorithm is robust with respect to noise and initial placement of the template on the image.

There are a number of places in the algorithm where modifications can be made. First, more sophisticated numerical techniques of conformal mapping may be considered. These are discussed in [7] and [21]. Second, it may be possible to create more elaborate criteria for constructing the orthogonal curves leading to nonconformal grids such as those discussed in [1], [12], [16] and [20]. The use of Riemannian manifolds may be an attractive alternative to conformal mapping [16]. On the other hand, a major complication in using nonconformal

mappings is that of establishing existence—it is often not clear if a particular class of nonconformal orthogonal grids can be constructed for all closed curves. Third, adaptive discretization strategies for forming the discrete grid can be explored. The current algorithm creates base points uniformly along the circumference of the template. In some situations it may be appropriate to adaptively sample the circumference so that there are more base points in the high curvature segments of the template.

Finally, efficient storage of templates in libraries and their quick retrieval can be considered. Initial results seem to indicate that classical techniques of indexing such as Kd-trees can be adapted for this purpose [15].

APPENDIX

Here, we will see that if the energy is independent of curve parameterization, and if the optimum deformed curve is close to the template, then the search for the optimum curve need be conducted only along the normal.

In the following discussion, the template is assumed to be available as arc length parameterized $C: t \rightarrow (x(t), y(t))$. If

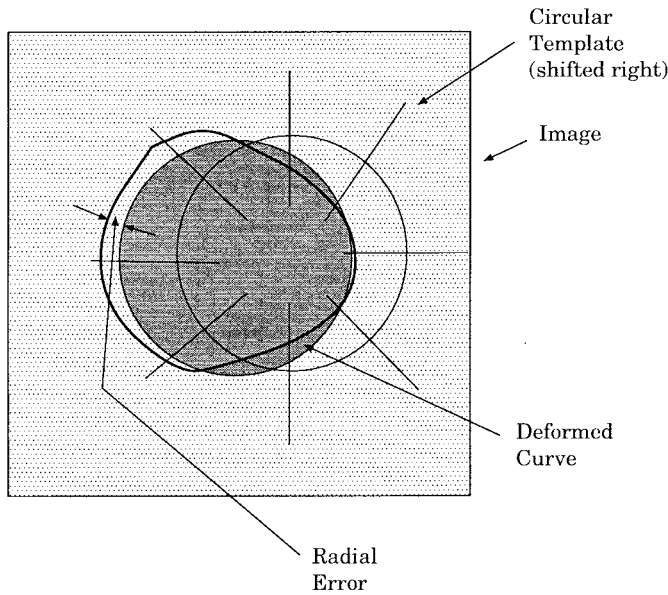


Fig. 12. Simulation.

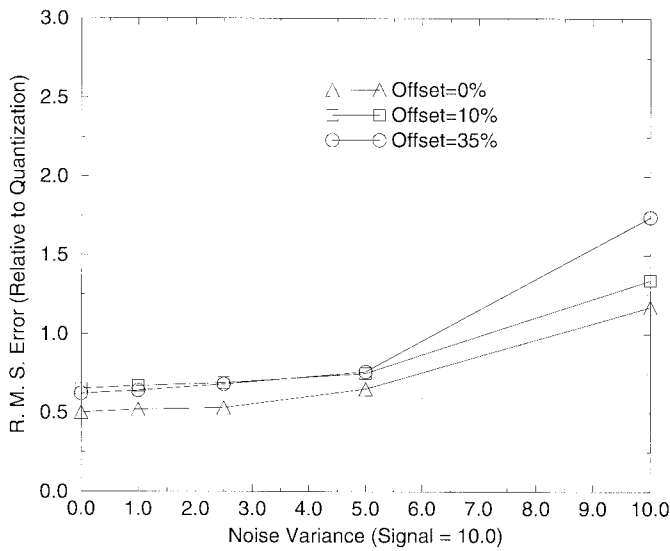


Fig. 13. Sensitivity to noise.

$(t_x(t), t_y(t))$ are the tangent vectors and $(n_x(t), n_y(t))$ the normal vectors to the curve, then any deformed curve can be expressed as

$$C^*: t \rightarrow \begin{pmatrix} \bar{x}(t) \\ \bar{y}(t) \end{pmatrix} = \begin{pmatrix} x(t) + \beta_1(t)t_x(t) + \beta_2(t)n_x(t) \\ y(t) + \beta_1(t)t_y(t) + \beta_2(t)n_y(t) \end{pmatrix}$$

for some functions $\beta_1(t)$ and $\beta_2(t)$. Since C^* is closed and continuous, $\beta_1(t), \beta_2(t)$ are periodic and continuous. We also assume that $\beta_1(t)$ and $\beta_2(t)$ have continuous derivatives and that $\max \beta_1(t)$ and $\max \beta_2(t)$ exist.

We shall see that when $\beta_1(t)$ and $\beta_2(t)$ are “small enough,” $\beta_1(t)$ has no effect on the energy, i.e., we will embed C^* in a family of curves C_{α_1, α_2}^* given by

$$C_{\alpha_1, \alpha_2}^*: t \rightarrow \begin{pmatrix} x(t) + \alpha_1 \beta_1(t)t_x(t) + \alpha_2 \beta_2(t)n_x(t) \\ y(t) + \alpha_1 \beta_1(t)t_y(t) + \alpha_2 \beta_2(t)n_y(t) \end{pmatrix}$$

TABLE III
RESULTS OF SIMULATION

X offset (%)	Noise (Signal=10)	R.M.S.Error (100 trials)
0.0	0.0	0.5
0.0	1.0	0.52
0.0	2.5	0.53
0.0	5.0	0.65
0.0	10.0	1.17
10.0	0.0	0.65
10.0	1.0	0.67
10.0	2.5	0.69
10.0	5.0	0.75
10.0	10.0	1.34
35.0	0.0	0.62
35.0	1.0	0.64
35.0	2.5	0.68
35.0	5.0	0.76
35.0	10.0	1.74

and show that

$$\frac{\partial E(C_{\alpha_1, \alpha_2}^*)}{\partial \alpha_1} = 0$$

at $\alpha_1 = \alpha_2 = 0$.

We begin by finding an expression for $\frac{\partial E(C_{\alpha_1, \alpha_2}^*)}{\partial \alpha_1}$ at $\alpha_1 = \alpha_2 = 0$. Since

$$E = \int \Gamma(\bar{x}(t), \bar{y}(t), \dot{\bar{x}}(t), \dot{\bar{y}}(t), \dots, \bar{x}^{(n)}(t), \bar{y}^{(n)}(t)) dt$$

we have

$$\begin{aligned} \left. \frac{\partial E}{\partial \alpha_1} \right|_{\alpha_1 = \alpha_2 = 0} &= \int \Gamma_x \frac{\partial \bar{x}}{\partial \alpha_1} + \Gamma_y \frac{\partial \bar{y}}{\partial \alpha_1} + \Gamma_{\dot{x}} \frac{\partial^2 \bar{x}}{\partial \alpha_1 \partial t} + \Gamma_{\dot{y}} \frac{\partial^2 \bar{y}}{\partial \alpha_1 \partial t} \\ &+ \dots + \Gamma_{x^{(n)}} \frac{\partial^{n+1} \bar{x}}{\partial \alpha_1 \partial t^n} + \Gamma_{y^{(n)}} \frac{\partial^{n+1} \bar{y}}{\partial \alpha_1 \partial t^n} \Big|_{\alpha_1 = \alpha_2 = 0} dt. \end{aligned}$$

But from the expression for C_{α_1, α_2}^* we have

$$\begin{aligned} \left. \frac{\partial \bar{x}}{\partial \alpha_1} \right|_{\alpha_1 = \alpha_2 = 0} &= \beta_1(t)t_x(t) \\ \left. \frac{\partial^{n+1} \bar{x}}{\partial \alpha_1 \partial t^n} \right|_{\alpha_1 = \alpha_2 = 0} &= \frac{d^n}{dt^n} \beta_1(t)t_x(t). \end{aligned}$$

Similarly

$$\begin{aligned} \left. \frac{\partial \bar{y}}{\partial \alpha_1} \right|_{\alpha_1 = \alpha_2 = 0} &= \beta_1(t)t_y(t) \\ \left. \frac{\partial^{n+1} \bar{y}}{\partial \alpha_1 \partial t^n} \right|_{\alpha_1 = \alpha_2 = 0} &= \frac{d^n}{dt^n} \beta_1(t)t_y(t). \end{aligned}$$

Thus

$$\begin{aligned} \left. \frac{\partial E(C_{\alpha_1, \alpha_2}^*)}{\partial \alpha_1} \right|_{\alpha_1 = \alpha_2 = 0} &= \int \left(\Gamma_x \beta_1(t)t_x(t) + \sum_{i=1}^n \Gamma_{x^{(i)}} \frac{d^i}{dt^i} (\beta_1(t)t_x(t)) \right) dt \\ &+ \int \left(\Gamma_y \beta_1(t)t_y(t) + \sum_{i=1}^n \Gamma_{y^{(i)}} \frac{d^i}{dt^i} (\beta_1(t)t_y(t)) \right) dt. \end{aligned}$$

This is the required expression. We now proceed to show that it is equal to zero.

This is done in the following way. C is embedded into another family of curves C_α , indexed by the variable α , and having the property that C_α is a continuous reparameterization of C when α is in a neighborhood of zero. Then, the expression $\frac{\partial E(C_\alpha)}{\partial \alpha}$ at $\alpha = 0$ is shown to be identical to the right-hand side of (14). Since C_α is just a reparameterization near $\alpha = 0$, and the energy is independent of parameterization, $\frac{\partial E(C_\alpha)}{\partial \alpha}$ must be zero. Thus, the expression on the right-hand side of (14) is zero.

The new family C_α is given by

$$C_\alpha : t \rightarrow \begin{pmatrix} x(t + \alpha\beta(t)) \\ y(t + \alpha\beta(t)) \end{pmatrix} = \begin{pmatrix} \hat{x}(t, \alpha) \\ \hat{y}(t, \alpha) \end{pmatrix}$$

where $\beta(t)$ is a continuous function with a continuous and bounded derivative. The function is specified below. We proceed by assuming that C_α is a continuous reparameterization in a neighborhood of $\alpha = 0$. The assumption is shown to hold below.

As before, we note that

$$\begin{aligned} \left. \frac{\partial^{k+1} \hat{x}(t, \alpha)}{\partial^{k+1} t \partial \alpha} \right|_{\alpha=0} &= \left. \frac{d^k}{dt^k} \left(\frac{\partial \hat{x}}{\partial \alpha}(t, \alpha) \right) \right|_{\alpha=0} \\ &= \frac{d^k}{dt^k} \beta(t) \dot{x}(t). \end{aligned}$$

Similarly

$$\left. \frac{\partial^{k+1} \hat{y}(t, \alpha)}{\partial^{k+1} t \partial \alpha} \right|_{\alpha=0} = \frac{d^k}{dt^k} \beta(t) \dot{y}(t).$$

Evaluating $\partial E(C_\alpha)/\partial \alpha$ we get

$$\begin{aligned} \left. \frac{\partial E(C_\alpha)}{\partial \alpha} \right|_{\alpha=0} &= \int \left(\Gamma_x \beta(t) \dot{x}(t) + \sum_{i=1}^n \Gamma_{x^{(i)}} \frac{d^i}{dt^i} \beta(t) \dot{x}(t) \right) dt \\ &+ \int \left(\Gamma_y \beta(t) \dot{y}(t) + \sum_{i=1}^n \Gamma_{y^{(i)}} \frac{d^i}{dt^i} \beta(t) \dot{y}(t) \right) dt. \end{aligned}$$

Noting that $\dot{x}(t) = t_x(t)$ and $\dot{y}(t) = t_y(t)$, and setting $\beta(t) = \beta_1(t)$ we see that

$$\left. \frac{\partial E(C_{\alpha_1, \alpha_2}^*)}{\partial \alpha_1} \right|_{\alpha_1 = \alpha_2 = 0} = \left. \frac{\partial E(C_\alpha)}{\partial \alpha} \right|_{\alpha=0}.$$

Now it remains to show that C_α is a continuous reparameterization of C near $\alpha = 0$. From the expression for C_α we see that it is sufficient to demonstrate that $t \rightarrow t + \alpha\beta(t)$ is a diffeomorphism near a neighborhood of $\alpha = 0$. The differential of the transformation is $1 + \alpha\dot{\beta}(t)$ and for $|\alpha| \leq \frac{1}{\max \beta(t)}$ the differential is invertible. Hence, there is

a neighborhood of $\alpha = 0$ for which the transformation is a continuous reparameterization.

ACKNOWLEDGMENT

The wrist images were supplied by G. Hillman of UTMB, Galveston, TX.

REFERENCES

- [1] A. Allievi and S. M. Calisal, "Application of Bubnov-Galerkin formulation to orthogonal grid generation," *J. Comput. Phys.*, vol. 98, pp. 163-173, 1992.
- [2] A. Amini, Tehrani, and T. E. Weymouth, "Using dynamic programming for minimizing the energy of active contours in the presence of hard constraints," in *Proc. 2nd Int. Conf. Comput. Vision*, 1988.
- [3] D. Ballard and C. Brown, *Computer Vision*. Englewood Cliffs, NJ: Prentice-Hall Inc., 1982.
- [4] J. F. Brinkley, "A flexible generic model for anatomical shape: Application to interactive two-dimensional medical image segmentation and matching," *Comput. Biomed. Res.*, vol. 26, pp. 121-142, 1993.
- [5] J. W. Bruce and P. J. Giblin, *Curves and Singularities*. Cambridge, UK: Cambridge Univ. Press, 1984.
- [6] W. E. L. Grimson, T. Lozano-Perez, W. M. Wells, III, and G. J. Ettinger, "An automatic registration method for frameless stereotaxy, image guided surgery, and enhanced reality visualization," in *Proc. Comput. Vision, Pattern Recog.*, 1994, pp. 430-436.
- [7] P. Henrici, *Applied and Computational Complex Analysis*. New York: Wiley, 1974.
- [8] M. Kass, A. Witkin, and D. Terzopoulos, "Snakes: Active contour models," *Int. J. Comput. Vision*, vol. 1, p. 321, 1988.
- [9] D. Kriegman and J. Ponce, "On recognizing and positioning curved 3-D objects from image contours," *IEEE Trans. Pattern Anal. Machine Intell.*, vol. 12, no. 12, Dec. 1990.
- [10] S. Kumar and D. Goldgof, "Automatic tracking of SPAMM grid and the estimation of deformation parameters from cardiac MR images," *IEEE Trans. Med. Imag.*, vol. 13, no. 1, Mar. 1994.
- [11] F. Leymarie and M. D. Levine, "Tracking deformable objects in the plane using active contour model," *IEEE Trans. Pattern Anal. Machine Intell.*, vol. 15, no. 6, June 1993.
- [12] J. W. Manke, "A tensor product B-spline method for numerical grid generation," *J. Comput. Phys.*, vol. 108, pp. 15-26, 1993.
- [13] Nehari, *Conformal Mapping*. New York: Dover, 1952.
- [14] C. Pelizzari, G. T. Chen, D. R. Spelbring, R. R. Weichselbaum, and C. T. Chen, "Accurate three-dimensional registration of CT, PET, and/or MRI images of the brain," *J. Comput. Assist. Tomogr.*, vol. 13, no. 1, pp. 20-26, 1989.
- [15] G. Robinson and H. D. Tagare, "Shape-based retrieval in medical image databases using KD-trees," *Div. Imag. Sci., Yale Univ., Tech. Rep. 95-2*, 1995.
- [16] G. Ryskin and L. G. Leal, "Orthogonal mapping," *J. Comput. Phys.*, vol. 50, pp. 71-100, 1983.
- [17] L. H. Staib and J. S. Duncan, "Boundary finding with parametrically deformable models," *IEEE Trans. Pattern Anal. Machine Intell.*, vol. 14, no. 11, Nov. 1992.
- [18] H. D. Tagare, K. W. Elder, D. M. Stoner, R. M. Patterson, C. L. Nicodemus, S. F. Viegas, and G. R. Hillman, "Location and geometric description of carpal bones in CT images," *Ann. Biomed. Eng.*, vol. 21, pp. 715-726, 1993.
- [19] H. D. Tagare, "Deformable 2-D template matching using orthogonal curves," *Div. Imag. Sci., Yale Univ., Tech. Rep. 95-4*, 1995.
- [20] J. F. Thompson, F. C. Thames, and C. W. Mastin, "Automatic numerical generation of body-fitted curvilinear coordinate system for field containing any number of arbitrary two-dimensional bodies," *J. Comput. Phys.*, vol. 15, pp. 299-319, 1974.
- [21] L. N. Trefethen, Ed., *Numerical Conformal Mapping*. New York: North-Holland, 1986.
- [22] Y. F. Wang and J. Wang, "Surface reconstruction using deformable models with interior and boundary constraints," *IEEE Trans. Pattern Anal. Machine Intell.*, vol. 14, no. 5, May 1992.
- [23] D. J. Williams and M. Shah, "A fast algorithm for active contours and curvature estimation," *CVGIP: Image Understanding*, vol. 55, no. 1, 1992.